SEMARAK ILMU PUBLISHING

Journal of Advanced Research in Fluid Mechanics and Thermal Sciences

Journal homepage:
https://semarakilmu.com.my/journals/index.php/fluid_mechanics_thermal_sciences/index
ISSN: 2289-7879

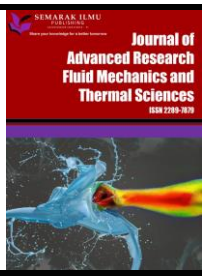

Numerical Study of Forced Convection Between Two Elliptical Cylinders with Variable ThermoPhysical Properties

Zerari Khalil[1], Haddad Zakaria[2,*]

[1] Department of Technical sciences, Institute of Science and Technology, Abdel Hafid Boussouf University, Mila, Algeria
[2] Department of Physics (Laboratory LPCM), Faculty of Sciences, Mohamed Boudiaf University, M'sila, Algeria

ARTICLE INFO

Article history:
Received 19 April 2022
Received in revised form 20 September 2022
Accepted 28 September 2022
Available online 21 October 2022

Keywords:
Forced convection; thermophysical properties; elliptical cylinders; finite volume; Fortran; Nusselt number

ABSTRACT

This study presents a numerical simulation of the three dimensional laminar forced convection between two elliptical horizontal cylinders with variable thermophysical properties using a program generated in FORTRAN language. The inner cylinder is uniformly heated whereas the outer cylinder is adiabatic. The flow and thermal fields are modeled by the continuity, momentum and energy equations with appropriate initial and boundary conditions using an elliptical coordinate system. The model equations are numerically solved by a finite volume numerical method with second order accurate spatiotemporal discretization. The variations of axial velocity, temperature and Nusselt number have been studied in three cases of forced convection, which are 100, 200 and 300 of Reynolds values. The results obtained show that the change in flow regime with increasing Reynolds number value has a significant effect on the value of Nusselt number, rather the heat exchange coefficient. Where Re=300 gives the best heat exchange.

1. Introduction

For the previous few decades, fluid dynamics and heat transfer have a lot of application in engineering and industries such as nuclear reactor, oil exploration, cosmetic products, wire drawing, construction equipment, electronic devices, heat exchangers and thermal power plants. [1-9]. Convection is the most common type of heat transfer in fluids, which are flows in/around various shapes [10-11], and the cylinders are considered one of the most widely used forms [12-16]. For this reason, the research on the convection heat transfer in cylinders has received special attention [17-23]. Lin Riyi *et al.,* [24] have studied the forced convection in a vertical eccentric ring with different ratios of radius and eccentricity (normalized by the difference in radius). Physical experiments and numerical simulations were carried out with a constant inner tube inlet temperature and hot water flow. The results show that with increasing radius ratios, the convective heat transfer coefficient increases, and for a radius ratio of 1.875, the heat transfer coefficient increases with increasing

* *Corresponding author.*
E-mail address: zakaria.haddad@univ-msila.dz

https://doi.org/10.37934/arfmts.100.1.96112

eccentricity. Othmane *et al.,* [25] have proposed a numerical study of coupled heat and mass transfer with phase change in an inclined channel. This channel is formed by two flat plates covered by a thin film of water and crossed by an ascending laminar flow of humid air. The plates are brought to a constant temperature (T_w) and to the corresponding saturation concentration (ω_w). The finite volume method was used to numerically solve the system of equations constituted by those of Navier-Stokes, energy and concentration. The velocity-pressure coupling is processed by the SIMPLER algorithm. The results show that the thermal and mass Archimedean forces detect the flow near the walls of the channel and thus induce a reversal of the latter. The magnitude of this reversal strongly depends on the angle of inclination of the channel. A rollover map was established for different angles of inclination. Jacques Charraudeau [26] is researching the influence of gradients of physical properties in forced convection application to the case of a tube. The system of dynamic and thermal boundary layer equations in the case of an incompressible flow with a linear initial velocity distribution and low variable physical property gradients was used. Dynamic viscosity and thermal conductivity were assumed to be a linear function of temperature. After explaining the relative variations of speed and temperature profiles resulting from the existence of variable physical properties, he specified the exact dependence of variations in wall friction and heat flux as a function of the Prandtl number, and he gave the contribution of each physical property gradient. Then, the author showed the possibilities of using the theoretical results by an application carried out in the case of the tube. Heat transfer rates for flow through a convergent-divergent channel have been analyzed by Wang and Chen [27] using a simple coordinate transformation method and the implicit Spline alternating direction method. The effects of wavy geometry, Reynolds number and Prandtl number on skin friction and Nusselt number were investigated. The results show that the amplitudes of Nusselt number and skin friction coefficient increase with increasing Reynolds number and amplitude-wavelength ratio. Mete Avcı and Orhan Aydın [28] analytically analyzed the heat transfer for forced convection in hydrodynamically and thermally fully developed flows of viscous dissipating gases in annular micro ducts between two concentric micro cylinders. Viscous dissipation effect, velocity slip and wall jump temperature are taken into consideration. Two different cases of thermal boundary conditions were considered. In the first, the heat flow is uniform at the outer wall and adiabatic to the inner wall, and in the second the heat flow is uniform at the inner wall and adiabatic to the outer wall. Solutions for velocity and temperature distributions and Nusselt number are obtained for different values of aspect ratio, and Knudsen and Brinkman numbers. Terhmina and Mojtabi [29] have numerically studied the laminar flow of forced convection at the entrance of an annular space, bounded by two coaxial and isothermal cylinders for unestablished velocity and temperature regimes. Fluid enters the annular space with uniform velocity and temperature. The results obtained with Peclet numbers, and ratios, radii, allow the correlation of heat transfer. Zerari Khalil [30] performed a numerical simulation on the effect of thermophysical properties on mixed convection in the annular space between two horizontal elliptical cylinders. The finite volume method with second-order spatio-temporal discretization was used to solve the modulus equations. It is concluded that consideration of mixed convection with varying physical properties gives physical meaning to flow and thermal fields that are qualitatively and quantitatively different from those of forced convection with temperature dependent properties and case of mixed convection with constant properties, the Nusselt number obtained is also higher in this case. The heat transfer enhancement obtained by considering natural convection within mixed convection with temperature-dependent physical properties increases with increasing Grashof number which is proportional to the heat flux imposed on the surface of the inner cylinder. The fluid thermophysical properties can influence the forced convection, which in turn affects fluid flow velocity and fluid temperature.

From the literature, there have been no previous studies of forced convection with low Reynolds, with the exception of Zerari Khalil study [30], but his work was limited for the forced convection only in Re=100. Therefore, this work shows the effect of low Reynolds (Re=100, 200 and 300) number in laminar forced convection. So, three cases of 3D laminar forced convection between two elliptical horizontal cylinders with variable thermophysical properties were numerically studied, which are 100, 200 and 300 of Reynolds values. The inner cylinder is uniformly heated whereas the outer cylinder is adiabatic. The flow and thermal fields are modeled and the equations are numerically solved by a finite volume method with second order accurate spatiotemporal discretization. The variations of axial velocity, temperature and Nusselt number have been presented and discussed.

2. Mathematical Formulation

2.1 Problem Description

We consider a forced convective flow in the annular space between two horizontal and concentric elliptical cylinders with variable properties. The inner cylinder is static and heated by a constant heat flux. The outer cylinder is static and adiabatic. The elliptical radii of the inner and outer cylinders are 0.5 and 1.0, respectively. The half-focal distance of the ellipses of the straight section of the duct is equal to 0.0045m. The length of the conduit is 100. At the inlet of the conduit, the fluid (water) has a constant axial velocity equal to (2.231 × 10-2 m/s for Re=100) (4.462 × 10-2 m/s for Re=200) (6.693 × 10-2 m/s for Re=300) and a uniform temperature equal to 20°C. A diagram of the problem is shown in Figure 1.

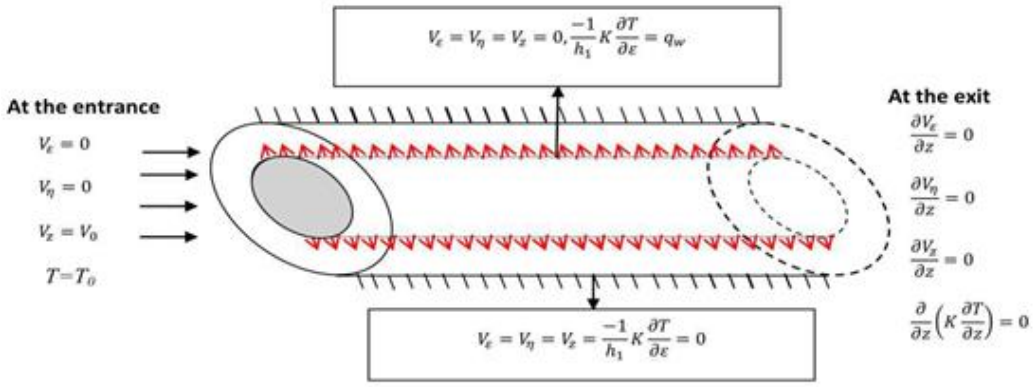

Fig. 1. Figure Geometry and boundary conditions of the problem

2.2 Table Style and Format

At t=0 we have

$$V_\varepsilon = 0, V_\eta = 0, V_z = 0, T = T_0$$

At t >0 we have the conservation equations

Continuity

$$\frac{1}{h_1 h_1}\left[\frac{\partial (h_2 V_\varepsilon)}{\partial \varepsilon} + \frac{\partial \left(h_1 V_\eta\right)}{\partial \eta} + \frac{\partial (h_1 h_2 V_z)}{\partial z}\right] = 0 \quad (1)$$

Momentum according to ε

$$\frac{\partial(\rho V_\varepsilon)}{\partial t}+\frac{1}{h_1h_2}\left[\frac{\partial(\rho h_2V_\varepsilon V_\varepsilon)}{\partial\varepsilon}+\frac{\partial\left(\rho h_1V_\eta V_\varepsilon\right)}{\partial\eta}+\frac{\partial(\rho h_1h_2V_zV_\varepsilon)}{\partial z}+\rho V_\varepsilon V_\eta\frac{\partial h_1}{\partial\eta}-\rho V_\eta^2\frac{\partial h_2}{\partial\varepsilon}\right]$$
$$=-\frac{1}{h_1}\frac{\partial P_h}{\partial\varepsilon}+\frac{1}{h_1h_2}\left[\frac{\partial}{\partial\varepsilon}\left(2\mu\frac{\partial V_\varepsilon}{\partial\varepsilon}\right)+\frac{\partial}{\partial\eta}\left(\mu\frac{\partial V_\varepsilon}{\partial\eta}\right)+\frac{\partial}{\partial z}\left(\mu h_1h_2\frac{\partial V_\varepsilon}{\partial z}\right)-2\mu\frac{1}{h_1h_2}V_\varepsilon\frac{\partial h_2}{\partial\varepsilon}\frac{\partial h_2}{\partial\varepsilon}\right.$$
$$+\frac{\partial}{\partial\varepsilon}\left(2\mu\frac{V_\eta}{h_1}\frac{\partial h_1}{\partial\eta}\right)-\frac{\partial}{\partial\eta}\left(\mu\frac{V_\varepsilon}{h_1}\frac{\partial h_1}{\partial\eta}\right)+\mu\frac{\partial}{\partial\varepsilon}\left(\frac{V_\eta}{h_2}\right)\frac{\partial h_1}{\partial\eta}+\mu\frac{\partial}{\partial\eta}\left(\frac{V_\varepsilon}{h_1}\right)\frac{\partial h_1}{\partial\eta}+\frac{\partial}{\partial z}\left(\mu h_2\frac{V_z}{\partial\varepsilon}\right)$$
$$\left.-2\mu\frac{1}{h_2}\frac{\partial V_\eta}{\partial\eta}\frac{\partial h_2}{\partial\varepsilon}+\frac{\partial}{\partial\eta}\left(\mu h_1\frac{\partial}{\partial\varepsilon}\left(\frac{V_\eta}{h_2}\right)\right)\right]+\rho ß(T-T_0)\frac{1}{\sqrt{h_1h_2}}cosh(\varepsilon)sin(\eta)g \quad (2)$$

Momentum according to η

$$\frac{\partial\left(\rho V_\eta\right)}{\partial t}+\frac{1}{h_1h_2}\left[\frac{\partial\left(\rho h_2V_\varepsilon V_\eta\right)}{\partial\varepsilon}+\frac{\partial\left(\rho h_1V_\eta V_\eta\right)}{\partial\eta}+\frac{\partial\left(\rho h_1h_2V_zV_\eta\right)}{\partial z}+\rho V_\varepsilon V_\eta\frac{\partial h_2}{\partial\varepsilon}\right.$$
$$\left.-\rho V_\varepsilon^2\frac{\partial h_1}{\partial\eta}\right] \quad (3)$$
$$=-\frac{1}{h_2}\frac{\partial P_h}{\partial\eta}+\frac{1}{h_1h_2}\left[\frac{\partial}{\partial\varepsilon}\left(\mu\frac{\partial V_\eta}{\partial\varepsilon}\right)+\frac{\partial}{\partial\eta}\left(2\mu\frac{\partial V_\eta}{\partial\eta}\right)+\frac{\eta}{\partial z}\left(\mu h_1h_2\frac{\partial V_\eta}{\partial z}\right)\right.$$
$$-2\mu\frac{1}{h_1h_2}V_\eta\frac{\partial h_1}{\partial\eta}\frac{\partial h_1}{\partial\eta}+\frac{\partial}{\partial z}\left(\mu h_1\frac{\partial V_z}{\partial\eta}\right)+\frac{\partial}{\partial\varepsilon}\left(\mu h_2\frac{\partial}{\partial\eta}\left(\frac{V_\varepsilon}{h_1}\right)\right)-\frac{\partial}{\partial\varepsilon}\left(\mu\frac{V_\eta}{h_2}\frac{\partial h_2}{\partial\varepsilon}\right)+\mu\frac{\partial}{\partial\varepsilon}\left(\frac{V_\eta}{h_2}\right)\frac{\partial h_2}{\partial\varepsilon}$$
$$\left.+\mu\frac{\partial}{\partial\eta}\left(\frac{V_\varepsilon}{h_1}\right)\frac{\partial h_2}{\partial e}-2\mu\frac{1}{h_1}\frac{\partial V_\varepsilon}{\partial\varepsilon}\frac{\partial h_1}{\partial\eta}+\frac{\partial}{\partial\eta}\left(2\mu\frac{V_\varepsilon}{h_2}\frac{\partial h_2}{\partial\varepsilon}\right)\right]+\rho ß(T-T_0)\frac{1}{\sqrt{h_1h_2}}sinh(\varepsilon)cos(\eta)g$$

Momentum according to z

$$\frac{\partial(\rho V_z)}{\partial t}+\frac{1}{h_1h_2}\left[\frac{\partial(\rho h_2V_eV_z)}{\partial\varepsilon}+\frac{\partial\left(\rho_0h_1V_\eta V_z\right)}{\partial\eta}+\frac{\partial(\rho_0h_1h_2V_zV_z)}{\partial z}\right]$$
$$=-\frac{\partial P_h}{\partial z}+\frac{1}{h_1h_2}\left[\frac{\partial}{\partial\varepsilon}\left(\mu\frac{\partial V_z}{\partial e}\right)+\frac{\partial}{\partial\eta}\left(\mu\frac{\partial V_z}{\partial\eta}\right)+\frac{\partial}{\partial z}\left(2\mu h_1h_2\frac{\partial V_z}{\partial z}\right)\right.$$
$$\left.+\frac{\partial}{\partial\varepsilon}\left(\mu h_2\frac{\partial V_\varepsilon}{\partial z}\right)+\frac{\partial}{\partial\eta}\left(\mu h_1\frac{\partial V_\eta}{\partial z}\right)\right] \quad (4)$$

Energy

$$C_p\frac{\partial(\rho T)}{\partial t}+C_p\frac{1}{h_1h_2}\left[\frac{\partial(\rho h_2V_\varepsilon T)}{\partial\varepsilon}+\frac{\partial\left(\rho h_1V_\eta T\right)}{\partial\eta}+\frac{\partial(\rho h_1h_2V_zT)}{\partial z}\right]$$
$$=\frac{1}{h_1h_2}\left[\frac{\partial}{\partial\varepsilon}\left(k\frac{\partial T}{\partial\varepsilon}\right)+\frac{\partial}{\partial\eta}\left(k\frac{\partial T}{\partial\eta}\right)+\frac{\partial}{\partial z}\left(kh_1h_2\frac{\partial T}{\partial z}\right)\right] \quad (5)$$

Initial and boundary conditions

t =0 $V_z = V_\eta = V_\varepsilon = 0,\ T = T_0$ *(Initial condition)*

$t > 0 \quad \varepsilon = 0.5, \quad V_z = V_\eta = V_\varepsilon = 0 \qquad q_w = -\frac{1}{h_1} k \frac{\partial T}{\partial \varepsilon}$ *(On inner cylinder wall)* (6)

$t > 0 \quad \varepsilon = 1, \quad V_z = V_\eta = V_\varepsilon = -\frac{1}{h_1} k \frac{\partial T}{\partial \varepsilon} = 0$ *(On outer cylinder wall)* (7)

$t > 0 \quad Z = 0, \quad V_z = V_0 \quad , V_\eta = V_\varepsilon = 0 \qquad T = T_0$ *(At conduit entrance)* (8)

$t > 0, \ \ z = L \ \ , \frac{\partial V_z}{\partial z} = \frac{\partial V_\eta}{\partial z} = \frac{\partial V_z}{\partial z} = \frac{\partial}{\partial z}\left(k \frac{\partial T}{\partial z}\right) = 0$ *(At conduit outlet)* (9)

Dimensionless variables and thermophysical properties are normalized by their characteristic scales to obtain dimensionless quantities which are presented in Table 1.

Table 1
Dimensionless thermophysical variables and properties

$h_1^* = \frac{h_1}{a} h_2^* = \frac{h_2}{a}$, $z^* = \frac{z}{a} t^* = \frac{V_0 t}{a}$, $V_\varepsilon^* = \frac{V_\varepsilon}{V_0} V_\eta^* = \frac{V_\eta}{V_0}$, $V_z^* = \frac{V_z}{V_0} T^* = \frac{T - T_0}{\frac{q_w a}{k_0}}$, $P^* = \frac{P - P_0}{\rho_0 V_0^2} \mu^* = \frac{\mu}{\mu_0}$, $k^* = \frac{K}{K_0} L^* = \frac{L}{a}$

2.3 Dimensionless Form of Mathematical Model Equations

Continuity

$$\frac{1}{h_1^* h_2^*}\left[\frac{\partial (h_2^* V_\varepsilon^*)}{\partial \varepsilon} + \frac{\partial \left(h_1^* V_\eta^*\right)}{\partial \eta} + \frac{\partial (h_1^* h_2^* V_z^*)}{\partial z^*}\right] = 0 \tag{10}$$

Momentum according to ε

$$\frac{\partial V_\varepsilon^*}{\partial t^*} + \frac{1}{h_1^* h_2^*}\left[\frac{\partial (h_2^* V_\varepsilon^* V_\varepsilon^*)}{\partial \varepsilon} + \frac{\partial \left(h_1^* V_\eta^* V_\varepsilon^*\right)}{\partial \eta} + \frac{\partial (h_1^* h_2^* V_z^* V_\varepsilon^*)}{\partial z^*} + V_\varepsilon^* V_\eta^* \frac{\partial h_1^*}{\partial \eta} - V_\eta^{*^2} \frac{\partial h_2^*}{\partial \varepsilon}\right]$$
$$= -\frac{1}{h_1^*} \frac{\partial P^*}{\partial \varepsilon} + \frac{1}{Re h_1^* h_2^*}\left[\frac{\partial}{\partial \varepsilon}\left(2\mu^* \frac{\partial V_\varepsilon^*}{\partial \varepsilon}\right) + \frac{\partial}{\partial \eta}\left(\mu^* \frac{\partial V_\varepsilon^*}{\partial \eta}\right) + \frac{\partial}{\partial z^*}\left(\mu^* h_1^* h_2^* \frac{\partial V_\varepsilon^*}{\partial z^*}\right) - 2\mu^* \frac{1}{h_1^* h_2^*} V_\varepsilon^* \frac{\partial h_2^*}{\partial \varepsilon} \frac{\partial h_2^*}{\partial \varepsilon}\right.$$
$$+ \frac{\partial}{\partial \varepsilon}\left(2\mu^* \frac{V_\eta^*}{h_1^*} \frac{\partial h_1^*}{\partial \eta}\right) - \frac{\partial}{\partial \eta}\left(\mu^* \frac{V_\varepsilon^*}{h_1^*} \frac{\partial h_1^*}{\partial \eta}\right) + \mu^* \frac{\partial}{\partial \varepsilon}\left(\frac{V_\eta^*}{h_2^*}\right) \frac{\partial h_1^*}{\partial \eta} + \mu^* \frac{\partial}{\partial \eta}\left(\frac{V_\varepsilon^*}{h_1^*}\right) \frac{\partial h_1^*}{\partial \eta} + \frac{\partial}{\partial z^*}\left(\mu^* h_2^* \frac{V_z^*}{\partial \varepsilon}\right)$$
$$\left. -2\mu^* \frac{1}{h_2^*} \frac{\partial V_\eta^*}{\partial \eta} \frac{\partial h_2^*}{\partial \varepsilon} + \frac{\partial}{\partial \eta}\left(\mu^* h_1^* \frac{\partial}{\partial \varepsilon}\left(\frac{V_\eta^*}{h_2^*}\right)\right)\right] + \frac{Gr}{Re^2} T^* \frac{1}{\sqrt{h_1^* h_2^*}} cosh(\varepsilon)\, sin(\eta) \tag{11}$$

Momentum according to η

$$\frac{\partial V_\eta^*}{\partial t^*}+\frac{1}{h_1^* h_2^*}\left[\frac{\partial\left(h_2^* V_\varepsilon^* V_\eta^*\right)}{\partial \varepsilon}+\frac{\partial\left(h_1^* V_\eta^* V_\eta^*\right)}{\partial \eta}+\frac{\partial\left(h_1^* h_2^* V_z^* V_\eta^*\right)}{\partial z^*}+V_\varepsilon^* V_\eta^* \frac{\partial h_2^*}{\partial \varepsilon}-V_\varepsilon^{*2} \frac{\partial h_1^*}{\partial \eta}\right]$$
$$=-\frac{1}{h_2^*}\frac{\partial P^*}{\partial \eta}+\frac{1}{\mathrm{Re}\, h_1^* h_2^*}\left[\frac{\partial}{\partial \varepsilon}\left(\mu^* \frac{\partial V_\eta^*}{\partial \varepsilon}\right)+\frac{\partial}{\partial \eta}\left(2\mu^* \frac{\partial V_\eta^*}{\partial \eta}\right)+\frac{\partial}{\partial z^*}\left(\mu^* h_1^* h_2^* \frac{\partial V_\eta^*}{\partial z^*}\right)-\right.$$
$$2\mu^* \frac{1}{h_1^* h_2^*} V_\eta^* \frac{\partial h_1^*}{\partial \eta}\frac{\partial h_1^*}{\partial \eta}+\frac{\partial}{\partial z^*}\left(\mu^* h_1^* \frac{\partial V_z^*}{\partial \eta}\right)+\frac{\partial}{\partial \varepsilon}\left(\mu^* h_2^* \frac{\partial}{\partial \eta}\left(\frac{V_\varepsilon^*}{h_1^*}\right)\right)-\frac{\partial}{\partial \varepsilon}\left(\mu^* \frac{V_\eta^*}{h_2^*}\frac{\partial h_2^*}{\partial \varepsilon}\right)+\mu^* \frac{\partial}{\partial \varepsilon}\left(\frac{V_\eta^*}{h_2^*}\right)\frac{\partial h_2^*}{\partial \varepsilon}$$
$$\left.+\mu^* \frac{\partial}{\partial \eta}\left(\frac{V_\varepsilon^*}{h_1^*}\right)\frac{h_2^*}{\partial \varepsilon}-2\mu^* \frac{1}{h_1^*}\frac{\partial V_\varepsilon^*}{\partial \varepsilon}\frac{\partial h_1^*}{\partial \eta}+\frac{\partial}{\partial \eta}\left(2\mu^* \frac{V_\varepsilon^*}{h_2^*}\frac{\partial h_2^*}{\partial \varepsilon}\right)\right]+\frac{Gr}{Re^2} T^* \frac{1}{\sqrt{h_1^* h_2^*}} sinh(\varepsilon)\, cos(\eta) \qquad (12)$$

Momentum according to z

$$\frac{\partial V_z^*}{\partial t^*}+\frac{1}{h_1^* h_2^*}\left[\frac{\partial(h_2^* V_\varepsilon^* V_z^*)}{\partial \varepsilon}+\frac{\partial\left(h_1^* V_\eta^* V_z^*\right)}{\partial \eta}+\frac{\partial(h_1^* h_2^* V_z^* V_z^*)}{\partial z^*}\right]$$
$$=-\frac{\partial P^*}{\partial z^*}+\frac{1}{Re h_1^* h_2^*}\left[\frac{\partial}{\partial \eta}\left(\mu^* \frac{\partial V_z^*}{\partial \varepsilon}\right)+\frac{\partial}{\partial \eta}\left(\mu^* \frac{\partial V_z^*}{\partial \eta}\right)+\frac{\partial}{\partial z^*}\left(2\mu^* h_1^* h_2^* \frac{\partial V_z^*}{\partial z^*}\right)\right.$$
$$\left.+\frac{\partial}{\partial \varepsilon}\left(\mu^* h_2^* \frac{\partial V_\varepsilon^*}{\partial z^*}\right)+\frac{\partial}{\partial \eta}\left(\mu^* h_1^* \frac{\partial V_\eta^*}{\partial z^*}\right)\right] \qquad (13)$$

Energy

$$\frac{\partial T^*}{\partial t^*}+\frac{1}{h_1^* h_2^*}\left[\frac{\partial(h_2^* V_\varepsilon^* T^*)}{\partial \varepsilon}+\frac{\partial\left(h_1^* V_\eta^* T^*\right)}{\partial \eta}+\frac{\partial(h_1^* h_2^* V_z^* T^*)}{\partial z^*}\right]$$
$$=\frac{1}{Re\, Pr\, h_1^* h_2^*}\left[\frac{\partial}{\partial \varepsilon}\left(k^* \frac{\partial T^*}{\partial \varepsilon}\right)+\frac{\partial}{\partial \eta}\left(k^* \frac{\partial T^*}{\partial \eta}\right)+\frac{\partial}{\partial z^*}\left(k^* h_1^* h_2^* \frac{\partial T^*}{\partial z^*}\right)\right] \qquad (14)$$

Initial and boundary conditions

$$t^*=0,\ V_\varepsilon^*=V_\eta^*=V_z^*=T^*=0 \qquad (15)$$

$$t^*>0,\ \varepsilon=0.5,\qquad V_\varepsilon^*=V_\eta^*=V_z^*=0,\qquad -\frac{1}{h_1^*}k^* \frac{\partial T^*}{\partial \varepsilon}=1 \qquad (16)$$

$$t^*>0,\ \varepsilon=1,\ V_\varepsilon^*=V_\eta^*=V_z^*=-\frac{1}{h_1^*}k^* \frac{\partial T^*}{\partial \varepsilon}=0 \qquad (17)$$

$$t^*>0,\qquad z^*=0,\ V_\varepsilon^*=V_\eta^*=0,\ V_z^*=1,\ T^*=0 \qquad (18)$$

$$t^*>0,\ z^*=L^*=100,\quad \frac{\partial V_\varepsilon^*}{\partial z^*}=\frac{\partial V_\eta^*}{\partial z^*}=\frac{\partial V_z^*}{\partial z^*}=\frac{\partial}{\partial z^*}\left(k^* \frac{\partial T^*}{\partial z^*}\right)=0 \qquad (19)$$

Some constants, reference values and control parameters (dynamic and thermal) are specified in Table 2.

Table 2
Thermophysical properties and control parameters

a	0.0045 m
g	9.81 m/s^2
β	1.8 × 10^{-4} /K
μ_0	1.006×10^{-3} kg/m.s
v_0	1.006 × 10^{-6} m^2/s
K_0	0.597 W/m · K
V_0	2.231 × 10^{-2} m/s,2× 2.231 × 10^{-2} m/s,3× 2.231 × 10^{-2} m/s
T_0	293 K
ρ_0	1000.52 kg/m^3
C_p	4182 J/kg · K

2.4 Modeling of Variable Physical Properties

Polynomial fittings, quite precise, to model the variations of viscosity and thermal conductivity with temperature. These fittings are precise to the following functions [19]

$$\mu(\mathrm{T}) = 1.79 \times 10^{-3} - 5.861 \times 10^{-5}(\mathrm{T} - 273.15) + 1.260 \times 10^{-6} \times (\mathrm{T} - 273.15)^2 - 1.736 \times 10^{-8}(\mathrm{T} - 273.15)^3 + 1.420 \times 10^{-10} \times (\mathrm{T} - 273.15)^4 - 6.177 \times 10^{-13}(\mathrm{T} - 273.15)^5 + 1.092 \times 10^{-15} \times (\mathrm{T} - 273.15)^6 \quad (20)$$

$$k(T) = -1.050 + 0.0108T - 2.172 \times 10^{-5}T^2 + 1.389 \times 10^{-8}T^3 \quad (21)$$

2.5 Finite Volume Method

The finite volume method consists in discretizing the physical domain under study into a computational domain which consists of a finite number of volumes. Each volume will be marked by a node and limited by six faces. Figure 2 illustrates a typical control volume. Point P at the center of the typical control volume is surrounded in each direction by two faces and two nodes in each direction.

For the radial direction, the points at the nodes are noted N, S and the faces are identified by n and s, and for the azimuthal direction, the points at the nodes are noted E, W and the faces are identified by e and w. Finally following the axial direction, the nodes are noted F, B and the faces are noted f, b.

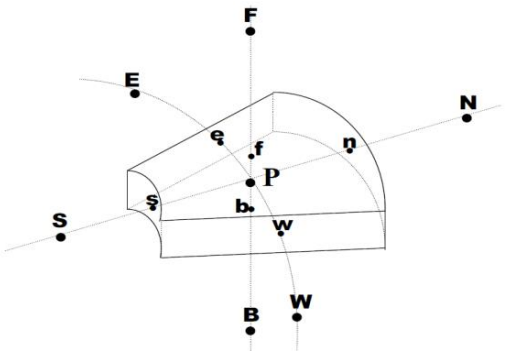

Fig. 2. Representation of finished volume

The mesh chosen for this study is schematically represented in Figure 3 It is composed of 32 points along the radial direction, 102 points along the axial direction and 85 points along the azimuthal direction. Any mesh denser than the one we used (32*102*85) exceeds the storage capacities of the best computers available to us and computation times that exceed practical durations. However, we think that our grid can be improved by a refinement, especially along the azimuthal and axial direction, to better discern important qualitative and quantitative variations of certain phenomena.

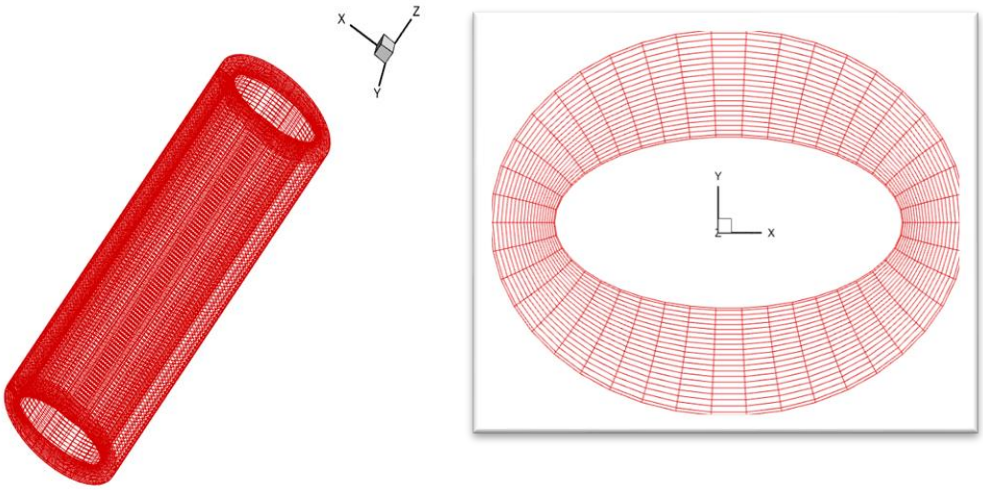

Fig. 3. The digital mesh used and its projection

3. Results

3.1 First Case For Re=100

3.1.1 Axial flow

This Figure 4 presents radial and angular variations of the axial velocity in the four axial positions which are : $Z^* = 25.5,\ Z^* = 50.5,\ Z^* = 75.5, Z^* = 100$. From the cylinder inlet $Z^* = 0$ until $Z^* = 22.5$ the flow develops uniformly in the axial direction and also there are variations along the other radial and azimuth directions. Boundary layers are formed on the inner wall of the outer cylinder and the outer wall of the inner cylinder, the thickness of this boundary layer increases axially. When we arrive at $Z^* = 50.5$ until the outlet, the secondary flow disappears after we obtain the hydrodynamic entrance length and the direction of flow deviates totally hydrodynamically developed axially. In the interval $Z^* = 22.5$ up to $Z^* = 100$ the two-dimensional flow and the axial velocity depend only on the two polar coordinates. The axial speed increases radially and reaches a maximum value at half the air gap between the inner cylinder wall and the outer cylinder, after exceeding half the air gap there is a decrease in speed through the outer cylinder wall. Following the azimuth direction, the speed increases in the counterclockwise direction and arrived at a maximum value at the point $\eta=\frac{\pi}{2}$ (this value is 1.89 at ε=0.775) after this point the speed decreases until η=π, and for the upper half-cylinder and by symmetry we have the same variation in the lower half-cylinder with respect to the horizontal axes.

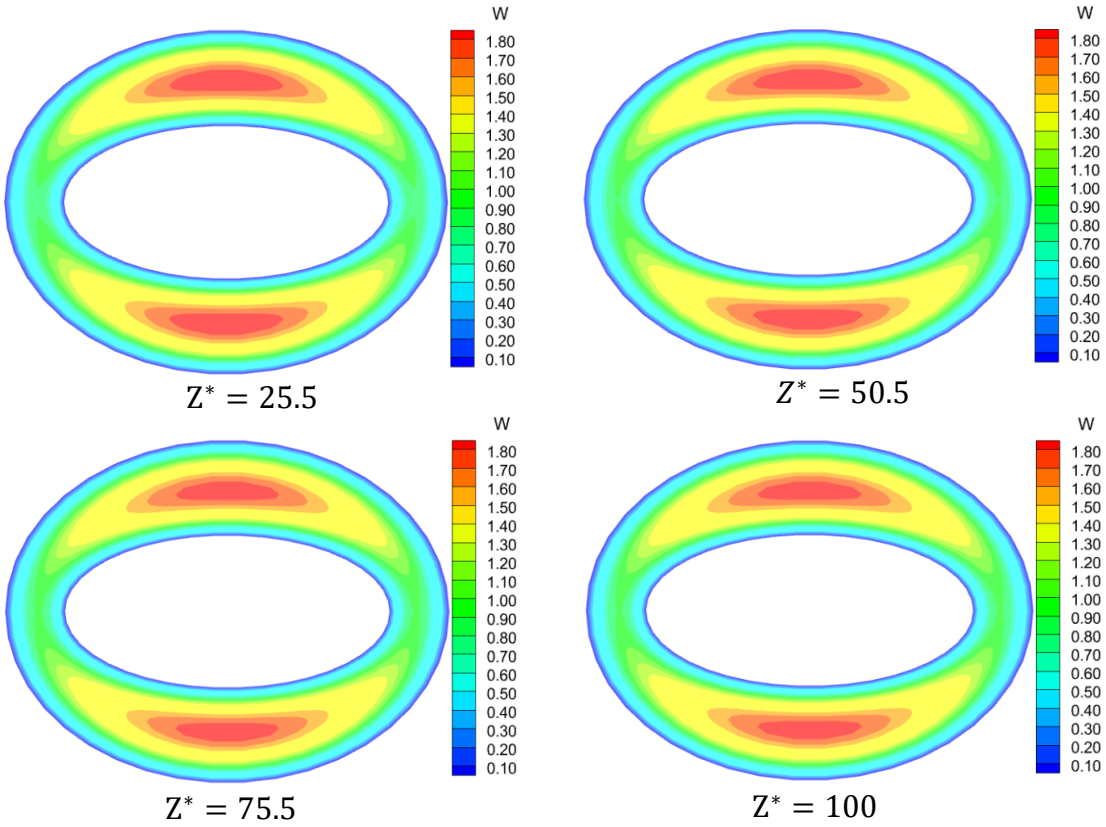

Fig. 4. Numerical field of the axial velocity at different value of Z* for Re=100

3.1.2 Thermal field

Figure 5 presents the thermal field variation in the case of Re=100 for four axial points chosen as follows (Z* = 25.5, z* = 50.5, Z*= 75.5, Z* = 100). The results illustrate that the thermal field increases axially from the cylinder inlet to the channel outlet because there is an addition of heat along the inner cylinder. The temperature is relatively high in the inner cylinder wall because there is parietal heating at the level of the latter, and with respect to the elliptical axes the thermal field is symmetrical. In the angular direction the temperature decreases from the elliptical horizontal axis to the vertical axis, and in the radial direction the temperature decreases from the inner cylinder wall to the outer cylinder wall.

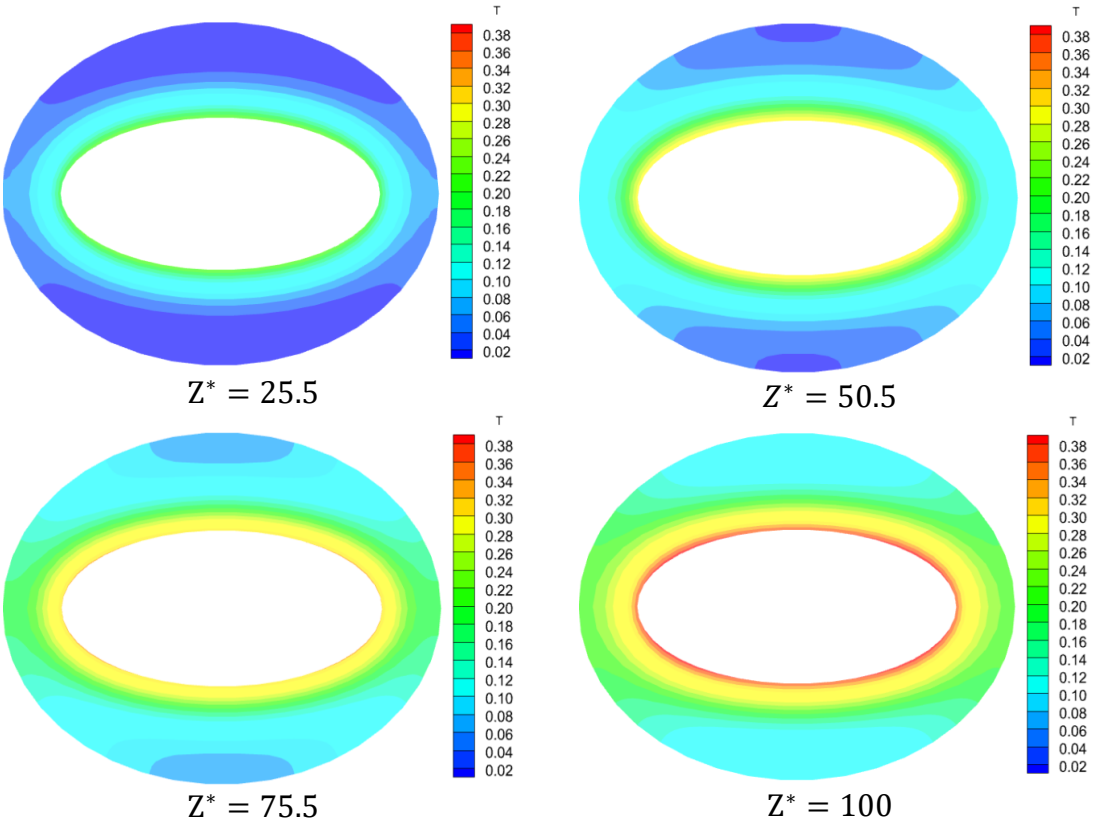

Fig. 5. Numerical field of the temperature at different values of Z* for Re=100

3.1.3 Nusselt number

Figure 6 presents the variation of axial Nusselt number for the case of Re=100. We can divide the curve into three parts, for the first part from Z*=0 to Z*=10 the value of the Nusselt number decreases rapidly from an initial value of about 26.02 to 7.15899. In the second part of Z*=10.5 until Z*=70.5, the value of the Nusselt number continues its decrease slowly and obtained a value of 5.20394 in the pointZ*=70.5. The rest is the third part, where the Nusselt number remains stable until exiting the channel with an approximate minimum value of 5.05825.

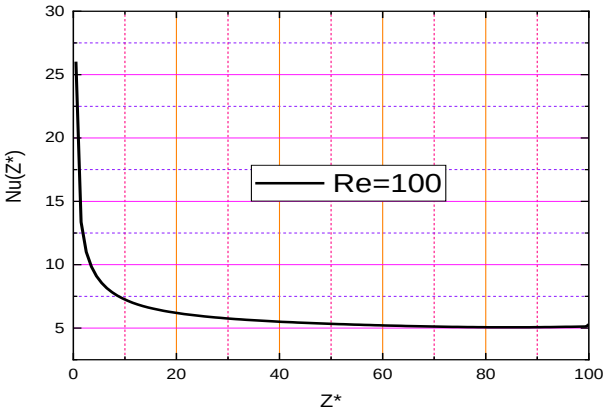

Fig. 6. Variation of axial Nusselt number as a function of Z* for Re=100

3.2 Second Case For Re=200

3.2.1 Axial flow

Figure 7 presents radial and angular variations of the axial velocity in the four axial positions (Z*=25.5,Z*=50.5,Z*=75.5,Z*=100). It is clear that we have a horizontal and vertical symmetry of the variation of the axial flow. For the interval Z*=0 until to Z*=44.5 the velocity starts its variation according to the three elliptical directions (axial, radial, azimuthal) starting from the channel entry. For axial direction the maximum velocity equal to 1.89 at the point (ε=0.775, η=π/2, Z=44.5), after this point the axial velocity variations are negligible until the cylinder outlet. Concerning radial direction, the velocity increases and obtains a maximum value in the half of the air gap, after which it begins its decrease towards the inner wall of the outer cylinder. For the azimuthal direction, the velocity increases from point η=0 and reaches a maximum value in η=π/2, then there is a decrease until η=π.

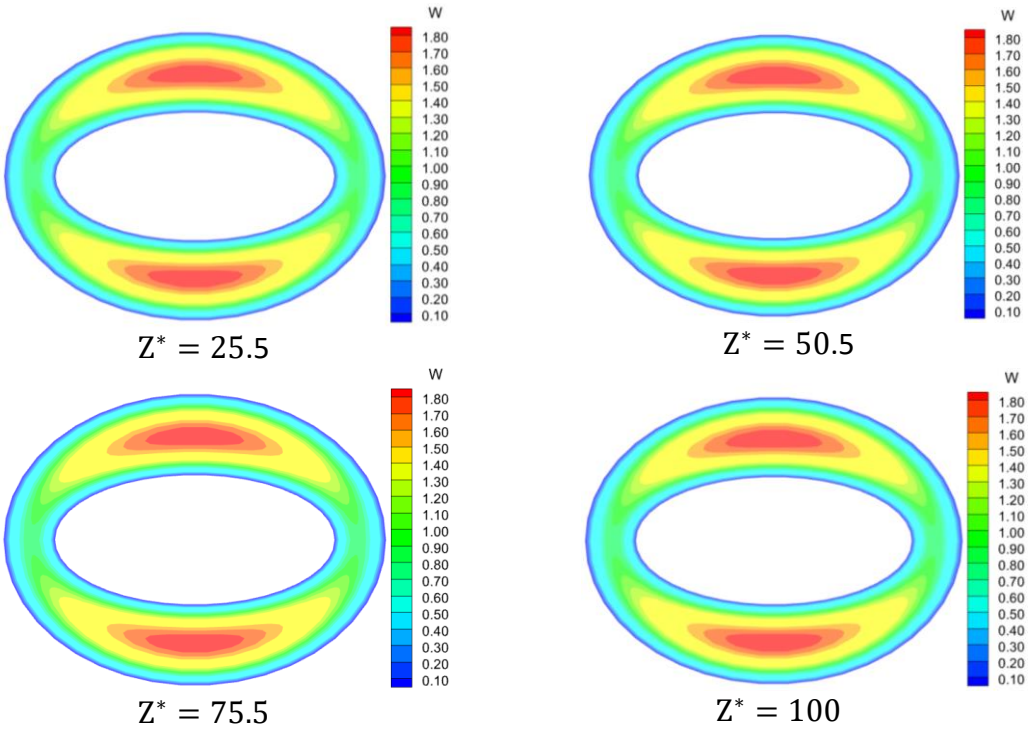

Fig. 7. Numerical field of the axial velocity at different value of Z* for Re=200

3.2.2 Thermal field

Figure 8 presents thermal field variations for the four axial points chosen as follows (Z* = 25.5, Z* = 45.5, Z*= 75.5, Z* = 100). The results show that the thermal field develops axially along the conduit, and the temperature increases radially from the inner cylinder (which is hot) towards the outer cylinder (adiabatic). The azimuthal variations are almost qualitatively identical to the case of Re=100. Concerning the axial variations, the temperature increases from the conduit inlet to the outlet, and it reaches a maximum value T_{max}=0.291 at the surface of the internal cylinder (Z=100).

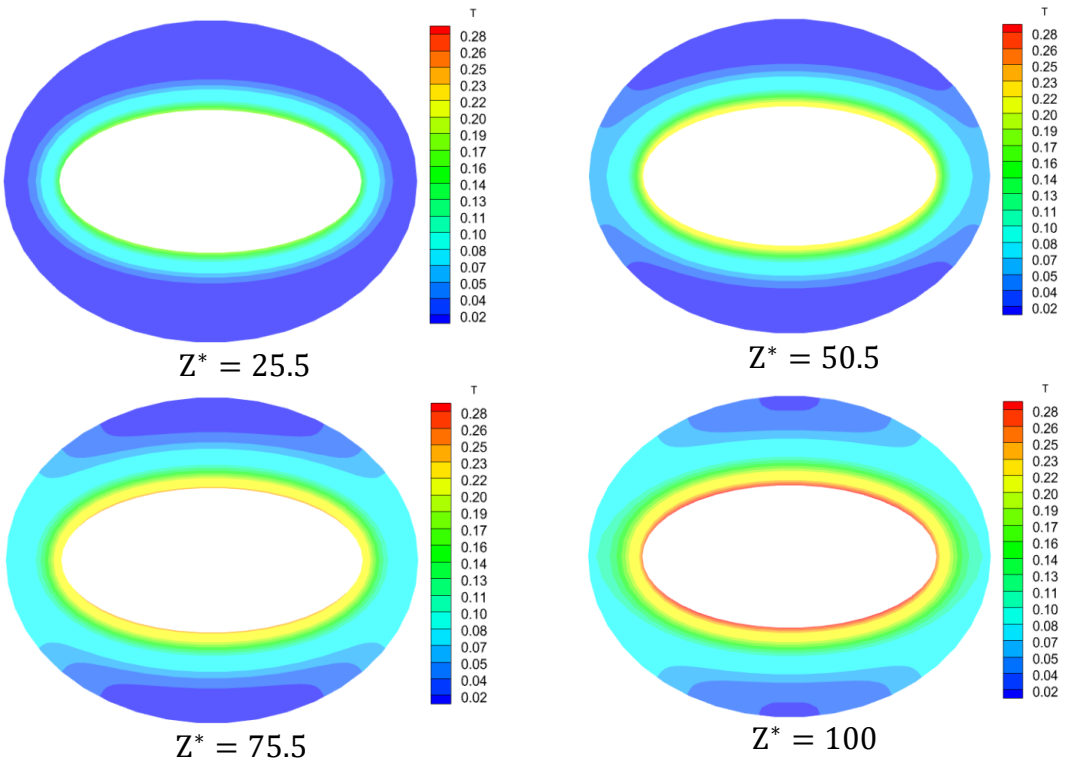

Fig. 8. Numerical field of the temperature at different values of Z* for Re=200

3.2.3 Nusselt number

Figure 9 presents the variations of the axial Nusselt number as a function of Z* for the case of Re=200. From the inlet to Z*=30.5 there is a large transfer between the inner cylinder wall and the fluid, and the value of Nu=6.45572 (Z*=30.5). After Z*=30.5 until the outlet of the conduit, the Nusselt number decreases slightly until the outlet of the conduit where its value at the outlet (Z*=100) Nu=5.37007.

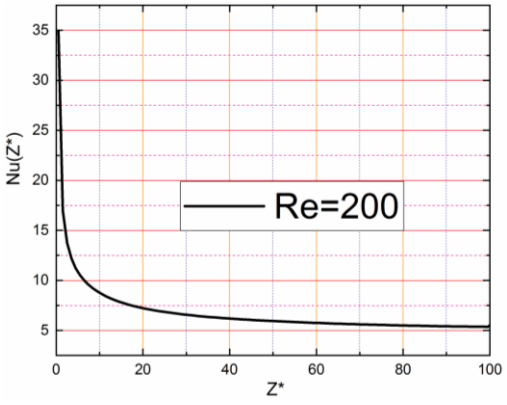

Fig. 9. Variation of axial Nusselt number as a function of Z* for Re=100

3.3 Third Case for Re=300
3.3.1 Axial flow

Figure 10 presents radial and angular variations of the axial velocity in the four axial positions (Z*=25.5,Z*=50.5, Z*=75.5,Z*=100). The results illustrate that there is horizontal and vertical

symmetry in the axial flow variation. For the interval Z*=0 up to Z*=50.5 the velocity begins its variation along the three elliptical directions (axial, radial, azimuthal) from the conduit inlet. For the axial direction the maximum velocity is about 1.89 at (ε=0.775, η=π/2, Z=50.5), after this point the axial velocity variations are negligible until the cylinder exit. Concerning the radial direction, the speed increases and reaches a maximum value in the half of the air gap, then it begins to decrease towards the inner wall of the outer cylinder. For the azimuth direction the velocity increases from point η=0 up to a maximum value for η=π/2, after which it is decreased up to η=π.

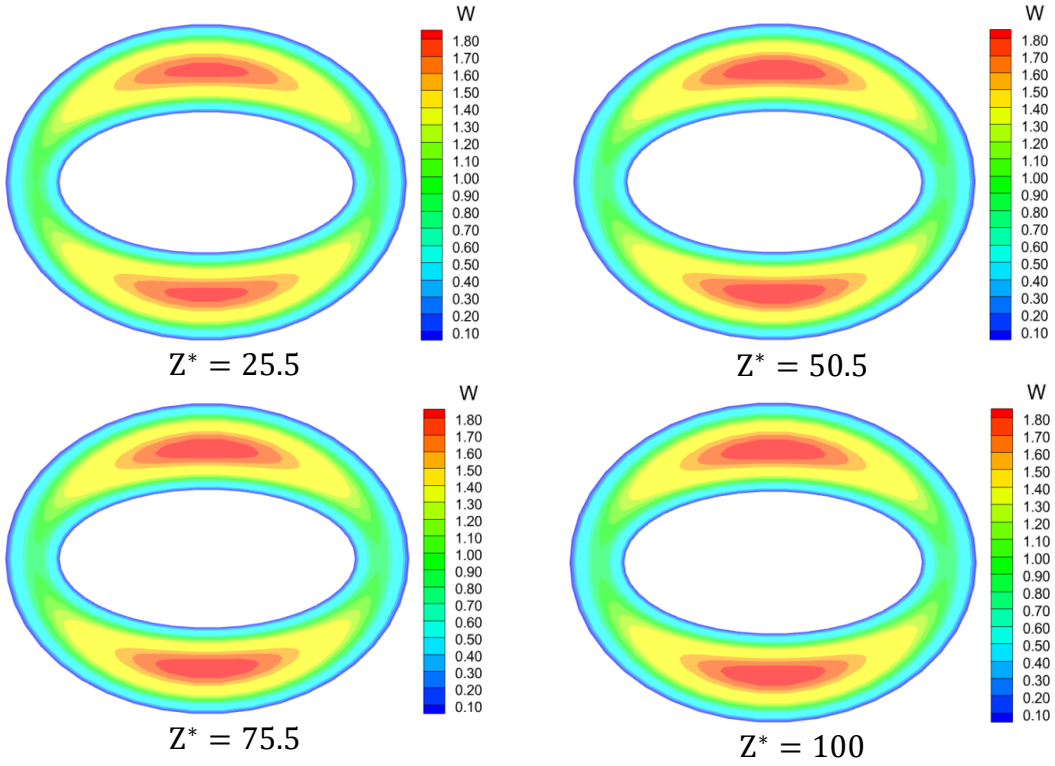

Fig. 10. Numerical field of the axial velocity at different value of Z* for Re=300

3.3.2 Thermal Field

Figure 11 presents thermal field variations in the case of Re=300 for four axial points chosen as follows (Z*= 25.5, Z* = 50.5, Z*= 75.5, Z* = 100). According to the results, the thermal field develops axially along the conduit. Also, the temperature increases radially from the inner cylinder (hot) to the outer cylinder (adiabatic). The azimuthal variations are almost qualitatively identical to the case of Re=100. Regarding axial variations, the temperature increases from the conduit inlet to the outlet, and it reaches a maximum value T_{max}=0.2412 at the cylinder internal surface (Z=100).

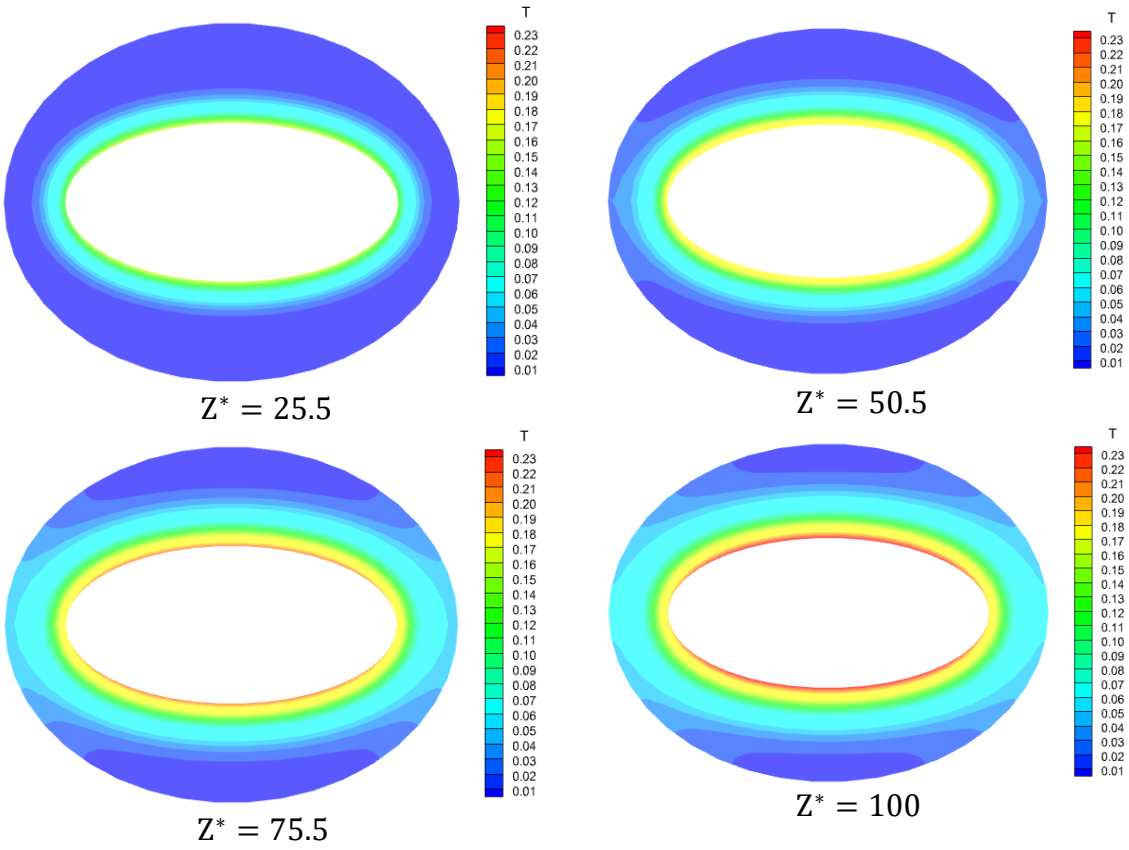

Fig. 11. Numerical field of the temperature at different values of Z* for Re=300

3.3.3 Nusselt number

The Figure 12 represents the variations of the axial Nusselt numbers Nu (Z*) for the following three Reynolds cases: Re=100, Re=200, Re=300. The diagrams can be divided into three parts. The first part of Z*=0 until Z*=10 the three diagrams decrease identically and quickly. After Z*=10 until Z*=40 there is a deceleration of the decrease, and for the last part of Z*=40 until the conduit exit the three graphs stabilize at certain value for each graph as follows: (Re=100, Nu=5.08933), (Re=200, Nu=5.36683), (Re=300, Nu=6.04825).

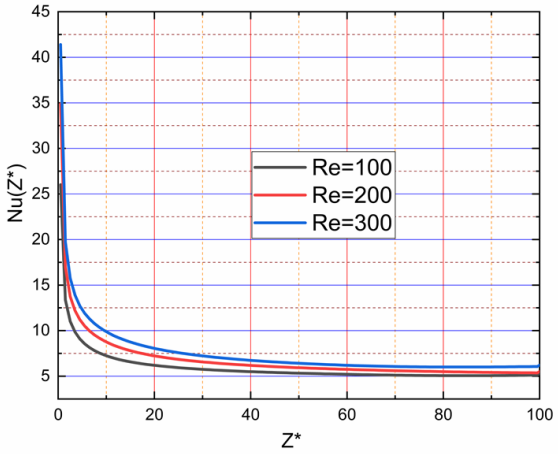

Fig. 12. Axial Nusselt numbers Nu (Z*) for different Reynolds number values

The values of different variables for the three calculation cases are grouped in the following Table 3.

Table 3
Values of different variables for the three calculation cases

	W_{max}	T_{max}	Nu_m	T_{ms}
Re=100	1.8935	0.3352	6.0153	0.1987
Re=200	1.8935	0.2911	6.8776	0.0993
Re=300	1.8935	0.2412	7.6256	0.0662

4. Conclusion

Numerical study of forced convection between two elliptical cylinders with variable thermophysical properties and comparison between three cases of forced convection has been presented. From the results achieved in the present research work, the following conclusions are arrived

i. The axial velocity variations are qualitatively and quantitatively identical for the three cases.
ii. The temperature variations are qualitatively identical but quantitatively the temperature decreases with the increase in Reynolds number.
iii. The increase in Reynolds number causes an increase in Nusselt number, and consequently an improvement in the heat transfer.

References

[1] Jahan, Sultana, M. Ferdows, Md Shamshuddin, and Khairy Zaimi. "Radiative mixed convection flow over a moving needle saturated with non-isothermal hybrid nanofluid." *Journal of Advanced Research in Fluid Mechanics and Thermal Sciences* 88, no. 1 (2021): 81-93. https://doi.org/10.37934/arfmts.88.1.8193

[2] Kanafiah, Siti Farah Haryatie Mohd, Abdul Rahman Mohd Kasim, Syazwani Mohd Zokri, and Mohd Rijal Ilias. "Combined Convective Transport of Brinkman-viscoelastic Fluid Across Horizontal Circular Cylinder with Convective Boundary Condition." *Journal of Advanced Research in Fluid Mechanics and Thermal Sciences* 89, no. 2 (2022): 15-24. https://doi.org/10.37934/arfmts.89.2.1524

[3] Makhatar, Nur Asiah Mohd, Marita Mohd Ali Lee, and Nur Lailatulladha Mohamad Fauzi. "Flow Reversal of Fully Developed Combined Convection in a Vertical Channel with Boundary Condition of a Third Kind." *Journal of Advanced Research in Fluid Mechanics and Thermal Sciences* 91, no. 1 (2022): 56-68. https://doi.org/10.37934/arfmts.91.1.5668

[4] Ali, I. R., Ammar I. Alsabery, Norhaliza Abu Bakar, and Rozaini Roslan. "Mixed Convection in a Lid-Driven Horizontal Rectangular Cavity Filled with Hybrid Nanofluid by Finite Volume Method." *Journal of Advanced Research in Fluid Mechanics and Thermal Sciences* 93, no. 1 (2022): 110-122. https://doi.org/10.37934/arfmts.93.1.110122

[5] Asghar, Adnan, Teh Yuan Ying, and Khairy Zaimi. "Two-Dimensional Magnetized Mixed Convection Hybrid Nanofluid Over a Vertical Exponentially Shrinking Sheet by Thermal Radiation, Joule Heating, Velocity and Thermal Slip Conditions." *Journal of Advanced Research in Fluid Mechanics and Thermal Sciences* 95, no. 2 (2022): 159-179. https://doi.org/10.37934/arfmts.95.2.159179

[6] Sakr, Ismail M., Wageeh A. El-Askary, Ashraf Balabel, and Kamal Ibrahim. "Numerical study on natural and forced convection in electrochemical cells." *CFD letters* 5, no. 3 (2013): 81-96.

[7] Tey, Wah Yen, and Hooi Siang Kang. "Power Loss in Straight Polygon Pipe via CFD Simulation." *Progress in Energy and Environment* 7 (2018): 1-10.

[8] Azmi, Mohd Irwan Mohd, Nor Azwadi Che Sidik, Yutaka Asako, Wan Mohd Arif Aziz Japar, Nura Muaz Muhammad, and Nadlene Razali. "Numerical Studies on PCM Phase Change Performance in Bricks for Energy-Efficient Building Application–A Review." *Journal of Advanced Research in Numerical Heat Transfer* 1, no. 1 (2020): 13-21.

[9] Rebhi, Redha, Younes Menni, Giulio Lorenzini, and Hijaz Ahmad. "Forced-Convection Heat Transfer in Solar Collectors and Heat Exchangers: A Review." *Journal of Advanced Research in Applied Sciences and Engineering*

Technology 26, no. 3 (2022): 1-15. https://doi.org/10.37934/araset.26.3.115

[10] Parvin, Salma, Rehena Nasrin, M. A. Alim, N. F. Hossain, and Ali J. Chamkha. "Thermal conductivity variation on natural convection flow of water–alumina nanofluid in an annulus." *International Journal of Heat and Mass Transfer* 55, no. 19-20 (2012): 5268-5274. https://doi.org/10.1108/HFF-11-2018-0628

[11] Salma Parvin , Rehena Nasrin, M.A. Alim, N.F. Hossain, Ali J. Chamkha. 2012. "Thermal conductivity variation on natural convection flow of water–alumina nanofluid in an annulus". *International Journal of Heat and Mass Transfer* 55:5268–5274. http://dx.doi.org/10.1016/j.ijheatmasstransfer.2012.05.035

[12] Chamkha, Ali J., T. Groşan, and I. Pop. "Fully developed free convection of a micropolar fluid in a vertical channel." *International Communications in Heat and Mass Transfer* 29, no. 8 (2002): 1119-1127. https://doi.org/10.1016/S0735-1933(02)00440-2

[13] Tayebi, Tahar, and Ali J. Chamkha. "Entropy generation analysis due to MHD natural convection flow in a cavity occupied with hybrid nanofluid and equipped with a conducting hollow cylinder." *Journal of Thermal analysis and Calorimetry* 139, no. 3 (2020): 2165-2179. https://doi.org/10.1007/s10973-019-08651-5

[14] Dogonchi, A. S., M. K. Nayak, Nader Karimi, Ali J. Chamkha, and D. Domiri Ganji. "Numerical simulation of hydrothermal features of Cu–H2O nanofluid natural convection within a porous annulus considering diverse configurations of heater." *Journal of Thermal Analysis and Calorimetry* 141, no. 5 (2020): 2109-2125. https://doi.org/10.1007/s10973-020-09419-y

[15] Raza, Jawad, Fateh Mebarek-Oudina, and Ali J. Chamkha. "Magnetohydrodynamic flow of molybdenum disulfide nanofluid in a channel with shape effects." *Multidiscipline Modeling in Materials and Structures* (2019):737-757. https://doi.org/10.1108/MMMS-07-2018-0133

[16] Tayebi, Tahar, and Ali J. Chamkha. "Free convection enhancement in an annulus between horizontal confocal elliptical cylinders using hybrid nanofluids." *Numerical Heat Transfer, Part A: Applications* 70, no. 10 (2016): 1141-1156. http://dx.doi.org/10.1080/10407782.2016.1230423

[17] Widodo, Basuki, Adhi Surya Nugraha, and Tri Rahayuningsih. "Numerical Solution of Mixed Convection MHD Viscous Fluid Flow on Lower Stagnation Point of a Sliced Magnetic Sphere." *Journal of Advanced Research in Fluid Mechanics and Thermal Sciences* 95, no. 1 (2022): 110-120. https://doi.org/10.37934/arfmts.95.1.110120

[18] Shafie, Sharidan, Mohamad Hidayad Ahmad Kamal, Lim Yeou Jiann, Noraihan Afiqah Rawi, and Anati Ali. "Quadratic Convective Nanofluid Flow at a Three-Dimensional Stagnation Point with the g-Jitter Effect." *Journal of Advanced Research in Fluid Mechanics and Thermal Sciences* 93, no. 2 (2022): 111-124. https://doi.org/10.37934/arfmts.93.2.111124

[19] Osman, Husna Izzati, Nur Fatihah Mod Omar, Dumitru Vieru, and Zulkhibri Ismail. "A Study of MHD Free Convection Flow Past an Infinite Inclined Plate." *Journal of Advanced Research in Fluid Mechanics and Thermal Sciences* 92, no. 1 (2022): 18-27. https://doi.org/10.37934/arfmts.92.1.1827

[20] Rosaidi, Nor Alifah, Nurul Hidayah Ab Raji, Siti Nur Hidayatul Ashikin Ibrahim, and Mohd Rijal Ilias. "Aligned Magnetohydrodynamics Free Convection Flow of Magnetic Nanofluid over a Moving Vertical Plate with Convective Boundary Condition." *Journal of Advanced Research in Fluid Mechanics and Thermal Sciences* 93, no. 2 (2022): 37-49. https://doi.org/10.37934/arfmts.93.2.3749

[21] Mopuri, Obulesu, Raghunath Kodi, Charankumar Ganteda, Ramu Srikakulapu, and Giulio Lorenzini. "MHD heat and mass transfer steady flow of a convective fluid through a porous plate in the presence of diffusion thermo and aligned magnetic field." *Journal of Advanced Research in Fluid Mechanics and Thermal Sciences* 89, no. 1 (2022): 62-76. https://doi.org/10.37934/arfmts.89.2.5675

[22] Ramzan, Muhammad, Zaib Un Nisa, Ahmad Shafique, and Mudassar Nazar. "Slip and Thermo Diffusion Effects on the Flow Over an Inclined Plate." *Journal of Advanced Research in Fluid Mechanics and Thermal Sciences* 94, no. 2 (2022): 13-28. https://doi.org/10.37934/arfmts.94.2.1328

[23] Sheikh, Nadeem Ahmad, Dennis Ling Chuan Ching, Hamzah Sakidin, and Ilyas Khan. "Fractional Model for the Flow of Brinkman-Type Fluid with Mass Transfer." *Journal of Advanced Research in Fluid Mechanics and Thermal Sciences* 93, no. 2 (2022): 76-85. https://doi.org/10.37934/arfmts.93.2.7685

[24] Riyi, Lin, Wang Xiaoqian, Xu Weidong, Jia Xinfeng, and Jia Zhiying. "Experimental and numerical study on forced convection heat transport in eccentric annular channels." *International Journal of Thermal Sciences* 136 (2019): 60-69. https://doi.org/10.1016/j.ijthermalsci.2018.10.003

[25] OULAID, Othmane, and Brahim BENHAMOU. "EFFET DE L'INCLINAISON SUR LES TRANSFERTS COUPLÉS DE CHALEUR ET DE MASSE DANS UN CANAL SOUMIS À DES CONDITIONS ASYMÉTRIQUES.".

[26] Charraudeau, J. "INFLUENCE OF PHYSICAL-PROPERTIES OF GRADIENTS IN FORCED CONVECTION-APPLICATION IN CASE OF TUBE." *International Journal of Heat and Mass Transfer* 18, no. 1 (1975): 87-95. https://doi.org/10.1016/0017-9310(75)90011-3

[27] Wang, C-C., and C-K. Chen. "Forced convection in a wavy-wall channel." *International Journal of Heat and Mass Transfer* 45, no. 12 (2002): 2587-2595. https://doi.org/10.1016/S0017-9310(01)00335-0

[28] Avcı, Mete, and Orhan Aydın. "Laminar forced convection slip-flow in a micro-annulus between two concentric cylinders." *International Journal of Heat and Mass Transfer* 51, no. 13-14 (2008): 3460-3467. https://doi.org/10.1016/j.ijheatmasstransfer.2007.10.036

[29] Terhmina, O., and A. Mojtabi. "FORCED-CONVECTION IN A HORIZONTAL ANNULAR SPACE FOR NON-ESTABLISHED VELOCITY AND TEMPERATURE REGIME." *International Journal of Heat and Mass Transfer* 31, no. 3 (1988): 583-590. https://doi.org/10.1016/0017-9310(88)90040-3

[30] Zerari, K., M. Afrid, and D. Groulx. "Forced and mixed convection in the annulus between two horizontal confocal elliptical cylinders." *International journal of thermal sciences* 74 (2013): 126-144.. https://doi.org/10.1016/j.ijthermalsci.2013.06.006